Technical Advances in Image Guidance of Radionuclide Therapy

Casper Beijst[1,2], Britt Kunnen[1,2], Marnix G.E.H. Lam[1], and Hugo W.A.M. de Jong[1]

[1]Department of Radiology and Nuclear Medicine, UMC Utrecht, Utrecht, The Netherlands; and [2]Image Sciences Institute, UMC Utrecht, Utrecht, The Netherlands

Internal radiation therapy with radionuclides (i.e., radionuclide therapy) owes its success to the many advantages over other, more conventional, treatment options. One distinct advantage of radionuclide therapies is the potential to use (part of) the emitted radiation for imaging of the radionuclide distribution. The combination of diagnostic and therapeutic properties in a set of matched radiopharmaceuticals (sometimes combined in a single radiopharmaceutical) is often referred to as theranostics and allows accurate diagnostic imaging before therapy. The use of imaging benefits treatment planning, dosimetry, and assessment of treatment response. This paper focuses on a selection of advances in imaging technology relevant for image guidance of radionuclide therapy. This involves developments in nuclear imaging modalities, as well as other anatomic and functional imaging modalities. The quality and quantitative accuracy of images used for guidance of radionuclide therapy is continuously being improved, which in turn may improve the therapeutic outcome and efficiency of radionuclide therapies.

Key Words: imaging; radionuclide therapy; theranostics; advances

Radionuclide therapy combines aspects of both chemotherapy (such as the cancer cell–targeting capabilities) and external-beam radiotherapy (by making use of ionizing radiation). An advantage of using radionuclide therapy over external-beam radiotherapy is that radionuclide therapy has the potential to eliminate not only the primary tumor but also metastasized or undetected tumors. Moreover, unlike chemotherapy, the radiopharmaceuticals used for radionuclide therapy potentially destroy adjacent tumor cells even if they lack specific uptake. Strategies for targeted delivery of radionuclides include binding of radionuclides to a cell-targeting molecule, such as treatment of neuroendocrine tumors with ^{177}Lu-DOTATATE (1); use of the ability of the radionuclide to target specific cells on its own, such

as the treatment of thyroid carcinoma with ^{131}I (2); and intraarterial injection, such as radioembolization with ^{90}Y microspheres for liver malignancies (3).

Another advantage of radionuclide therapies is the potential to use the emitted radiation for imaging of the radionuclide distribution. The combination of diagnostic and therapeutic properties in a set of matched radiopharmaceuticals (sometimes combined in a single radiopharmaceutical) is often referred to as theranostics and allows accurate diagnostic imaging before therapy. The use of imaging benefits treatment planning, dosimetry, and assessment of treatment response. Therefore, developments in imaging technologies may also benefit the efficacy of radionuclide therapies. This paper focuses on the technical developments in imaging technology relevant for imaging of radionuclide therapy. Developments in the field of the traditional nuclear imaging modalities (i.e., scintigraphy/SPECT and PET), as well as other anatomic and functional imaging modalities, are discussed.

SPECT AND SCINTIGRAPHY

The type of decay of radionuclides used for nuclear medicine therapy or its guidance determines what modality is used for imaging. Planar scintigraphy or SPECT is used for imaging of radionuclides—such as ^{177}Lu, ^{90}Y, and ^{131}I—that are used for radionuclide therapy. These nuclides emit γ-photons (or bremsstrahlung photons), which can be imaged with a γ-camera.

Current Status

Modern SPECT/CT systems can be used for planar as well as tomographic imaging. Planar imaging is readily used to acquire whole-body images in a limited amount of time, because imaging the whole body with a tomographic (SPECT) method would be time-consuming. SPECT is used to acquire 3-dimensional data to discern structures that would overlap one another on planar images. Planar and tomographic images are often acquired in sequence to obtain whole-body images in addition to 3-dimensional images of a specific part of the body.

Quantitative SPECT images can be obtained by converting the acquired counts into a distribution of absorbed dose (in Gy), which can benefit planning and dosimetry of radionuclide therapy. However, because of effects such as photon attenuation, scatter, and blurring, SPECT/CT
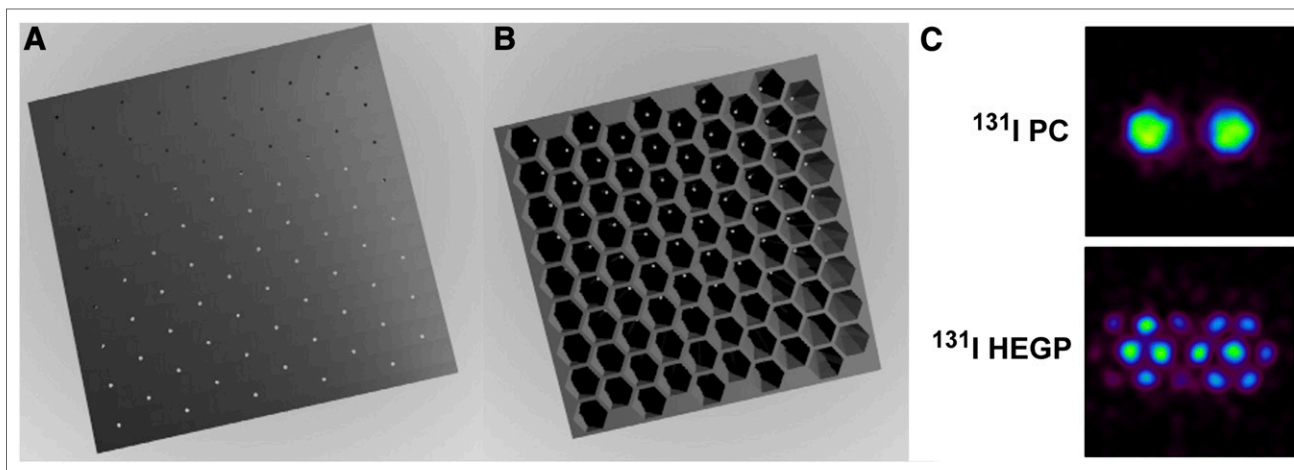
FIGURE 1. Face (A) and back (B) of parallel-cone (PC) collimator. (C) Double-point-source Monte Carlo simulations obtained for ^{131}I on PC collimator and high-energy general-purpose (HEGP) collimator. PC collimator can detect the 2 sources separately, whereas HEGP collimator cannot. (Reprinted from (8).)

images are not inherently quantitative. Attenuation correction is commonly incorporated in the projection operators of the iterative reconstruction method using attenuation maps from coregistered CT images. Scatter correction is also routinely implemented into clinical practice and is often performed using the triple-energy window method (4). Image quality can be further improved by applying resolution recovery. This is done by accurately characterizing the shape of the point-spread function, which depends on the distance from the camera and is rotationally variant because of the hexagonal pattern of the collimator septa. The point-spread function model can subsequently be incorporated into the reconstruction algorithm (5).

Even though image-degrading effects such as attenuation, scatter, and blurring can be partially corrected for, SPECT images suffer from partial-volume effects and quantification errors.

Advances in SPECT and Scintigraphy

This section discusses SPECT developments improving image quality in general, as well as those improving guidance of radionuclide therapy.

Instrumentation: Collimators and Detectors. Tumor dosimetry requires accurate quantification of small structures. This is severely hampered by the partial-volume effects that, by limiting image resolution, reduce contrast. Because image resolution is largely determined by collimator resolution, development of collimators that are less easily penetrated is one strategy to reduce partial-volume effects. Because many of the isotopes used for radionuclide therapies (e.g., ^{131}I and ^{90}Y) emit high-energy photons that easily penetrate the collimator and reduce image resolution, optimizing the collimator may be crucial to achieving quantitative accuracy. The strategy used to optimize parallel-hole collimators for high-energy applications is to increase septal thickness and

length to limit septal penetration. However, optimizing the design of a parallel-hole collimator involves a trade-off between septal penetration, spatial resolution, and sensitivity. Alternatively, one can use pinhole collimators designed to limit collimator penetration (6). However, quantitative pinhole SPECT remains a challenge in clinical practice for the following reasons: (1) truncated projections may lead to reconstruction artifacts, (2) dedicated software may be required for quantitative imaging, and (3) the sensitivity of pinhole collimators is limited. Multiple pinholes can be used to overcome the problem of limited sensitivity (7). Image quality may also be improved using a collimator consisting of cone-shaped holes (the parallel-cone collimator; Fig. 1), which limit collimator penetration while preserving resolution and sensitivity (8).

Detectors can be optimized for high-energy photons (emitted by the isotopes used for radionuclide therapies) using thicker crystals ($^5/_8$ inch instead of the standard $^3/_8$ inch) or using scintillation crystals with high stopping power, which increases the detection efficiency. Walrand et al. have designed a camera dedicated for Bremsstrahlung imaging of ^{90}Y (6). They describe a dedicated system with a 30-mm-thick bismuth germanate crystal and an 8-mm high-energy pinhole with extra shielding to prevent penetration of high-energy photons. Additionally, it is suggested that the camera can be mounted on a robotic gantry for use in the intervention room, as shown in Figure 2.

Advances in detector technology also include the development of solid-state detectors (9). Cadmium-zinc-telluride (CZT) detectors directly convert the energy of incident γ-photons into an electric signal, in contrast to indirect scintillation-based detector systems that require photomultiplier tubes. Advantages of CZT detectors are the high energy resolution and the high counting rate capability as compared with photomultiplier cameras with NaI
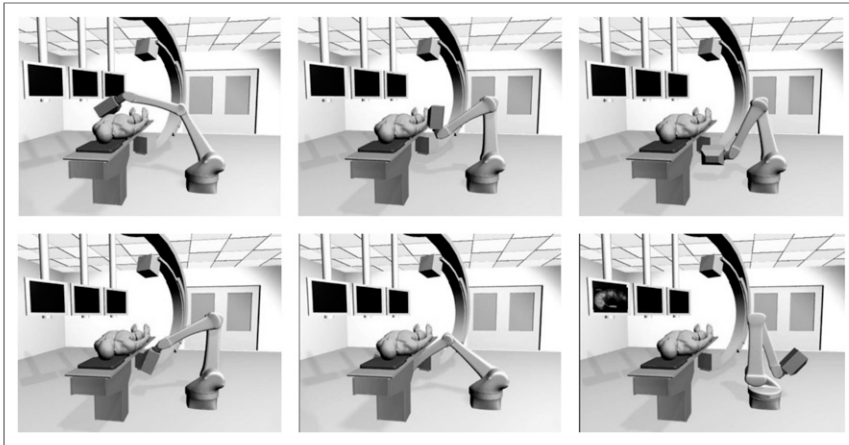
FIGURE 2. Interventional pinhole SPECT camera mounted on 6-axis arm robot (58). The images show how the robotic gantry is able to acquire tomographic images from multiple angles.

crystals. Superior energy resolution results in a lower detection of scattered events due to a narrow energy window. This advantage also paves the way for dual-isotope applications, for which clear separation of photopeaks is essential (10). The fact that CZT detectors can detect high count rates is an advantage for radionuclide therapies, as high activities are generally used to deliver the therapeutic radiation dose. However, CZT detectors have low stopping power, which makes them less suitable for imaging of high-energy photons. CZT technology is more suitable for isotopes with low-energy photopeaks, such as ^{99m}Tc, ^{166}Ho, or ^{177}Lu (11).

Reconstruction Algorithms. Specifically, for the application of radionuclide therapy, quantitative results benefit dosimetry and assessment of treatment response. However, iterative reconstruction algorithms are able to obtain images with a high signal-to-noise ratio but do not necessarily generate (linearly) quantitative images. In general, SPECT images have long been regarded as solely qualitative images, in contrast to PET, which allows the use of semiquantitative or quantitative measures such as the SUV. Despite the relatively low resolution of SPECT images (as compared with PET), quantitative SPECT images can now be obtained when image-degrading effects are adequately corrected for. These corrections include those for attenuation, scatter, point-spread function, or dead time. Although quantitative images can be obtained using easy-to-implement scatter correction techniques, the accuracy of quantitation can be improved using Monte Carlo–based scatter modeling (12). Monte Carlo–simulated forward projections can be used in the reconstruction algorithm to accurately model object scatter and, hence, correct for the image-degrading effects of scatter. Over the years, several Monte Carlo codes have been incorporated into the reconstruction algorithm, such as GATE, SIMSET, MCNP, SIMIND, and UMCS (13). Because Monte Carlo simulations are notoriously slow, acceleration is often performed using variance reduction techniques. One of the strategies is to use convolution-forced detection, which forces particles toward the collimator by creating daughter particles at every interaction in the phantom with weighting to correct for the likelihood of detection (14,15). Despite the challenges of quantitative SPECT, a quantitative accuracy of within 5% can be obtained, which is equivalent to the accuracy of PET/CT systems (16).

Quantitative images may be used for dosimetric applications in radionuclide therapy. Obtaining these images is not straightforward, because the acquired projection images are measured in counts. These can be converted into quantitative images representing the activity concentration (in Bq/unit volume) using quantitative reconstruction algorithms. In turn, quantitative images that represent patient dose (in Gy) may be obtained by taking into account an estimation of the retention time, the specific energy released and absorbed, and information about the spatial dose distribution (e.g., dose point kernels). The retention time may be estimated by assuming a theoretic effective half-life or by acquiring multiple scans over time to achieve a time-integrated activity in a target volume (organ or tumor). Subsequently, the absorbed dose can be calculated by multiplying the activity concentration by a radionuclide-specific constant (17), by convolving the activity distribution with a dose point kernel, or by performing Monte Carlo simulations (18), depending on the required accuracy of the dose estimation.

Advances in the development of SPECT reconstruction algorithms also involve the use of anatomic priors. For example, maximum a posteriori algorithms that incorporate smoothing within, but not across, organ or lesion boundaries may improve the quality of images used for guidance of radionuclide therapy (19). A fundamental issue with anatomic priors is that the resulting images are no longer purely molecular but also include anatomic information.

Developments in SPECT reconstruction algorithms also include corrections for cardiac or respiratory motion (20). The correction for cardiac motion mostly benefits cardiac applications, whereas corrections for respiratory motion may improve lesion detection in general. Motion correction is discussed in more detail in the next section.

PET

^{18}F-FDG PET accounts for most PET studies in clinical practice and is often used for staging and follow-up after radionuclide therapy. However, PET is also used for imaging of other nuclides (e.g., ^{90}Y, ^{124}I, ^{64}Cu, and ^{68}Ga) for treatment planning, dosimetry, and assessment of treatment response in radionuclide therapies. In all cases, good

quantitative accuracy is required, either for precise SUV-based therapy response monitoring or more detailed dosimetry for therapy planning.

Current Status

Like SPECT, quantitative PET requires application of correction techniques. Attenuation correction for PET can easily be performed by determining the attenuation correction sinogram, typically based on coregistered CT data. In addition, scatter correction is often implemented in clinical practice using the single-scatter simulation method (21). Correction for random counts is generally performed by applying delayed-event subtraction (22).

The time difference in detection between annihilation photons provides information about the location of the annihilation event along the line of response. This time-of-flight information can be incorporated in the reconstruction during the backprojection step to improve image quality. The availability of time-of-flight estimation has paved the way for imaging isotopes with very low positron abundance, such as ^{90}Y.

Because the intrinsic resolution of PET detectors is limited, the shape of the point-spread function can be incorporated in the reconstruction method to improve the quality of reconstructed images. This process is often referred to as resolution recovery.

Radiation detection systems suffer from dead-time effects due to pulse pile-up when subjected to high counting rates. Dead-time losses are routinely corrected for, based on measurements of a large range of activities and knowledge of the true counting rate model.

Advances

The quality of PET images is continuously being improved by advances in PET instrumentation and reconstruction aimed at increasing resolution and sensitivity, which in turn allows a more accurate determination of the SUV. Using nuclides such as ^{124}I and ^{90}Y, such improvements may aid in optimized targeting, treatment planning, dosimetry, and assessment of treatment response in radionuclide therapies.

Instrumentation. PET scanners traditionally use photomultiplier tubes to convert the optical signal coming from the scintillation crystal into an electronic signal. However, semiconductor-based alternatives are also becoming commercially available for clinical systems. The most commonly used alternatives are avalanche photodiodes and silicon photomultipliers (SiPMs). Avalanche photodiodes essentially are semiconductor photodetectors that operate in avalanche mode, which means that the output is linear with the amount of scintillation light. SiPMs consist of a multipixel array of small avalanche photodiodes that operate in Geiger mode. Therefore, the output of a single pixel of an SiPM is not linear with the amount of scintillation light. However, the number of SiPM pixels that produce an avalanche pulse is a measure of the energy of the incident γ-photon. The individual SiPM pixels have a size of 20–100 μm. SiPMs can be fabricated to couple with smaller
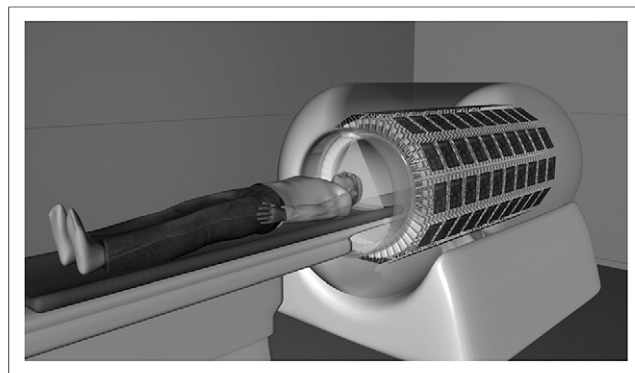

FIGURE 3. Explorer total-body PET scanner. (Courtesy of Drs. Simon R. Cherry and Ramsey D. Badawi, University of California, Davis.)

crystals and therefore improve resolution (23). Another advantage of SiPMs is their good timing resolution, which improves the signal-to-noise ratio of PET images (24,25) through better time-of-flight estimation.

Increasing the timing resolution enhances the time-of-flight estimation and, consequently, the signal-to-noise ratio of the images (24). Therefore, improvement of the timing resolution is subject to research. Time-of-flight detectors typically use $4 \times 4 \times 22$ mm scintillation crystal elements, with photodetectors placed on the top of the crystal element for readout. Moses et al. developed a detector in which the photodetector is mounted on the side of the crystal element (26). This design reduces the mean path length of the scintillation photons to the photodetectors, which in turn improves timing resolution. Another approach to improving the timing resolution is double-sided readout, as described by Seifert and Schaart (27). They describe a setup in which photodetectors are mounted on the top and bottom of the crystal element, enabling correction of depth-dependent effects to the timing uncertainty. An additional advantage of this approach is that depth of interaction can be extracted.

Another method to improve the efficiency of PET images is by increasing axial detector length. The image quality of low-abundance isotopes such as ^{90}Y may benefit from this approach. Extending the axial field of view of a PET scanner from 16.2 cm (3 detector rings) to 21.8 cm (4 detector rings) already significantly increases system sensitivity (28). A whole-body PET system with an axial detector length of approximately 2 m is currently under development at the University of California, Davis, as shown in Figure 3 (29). Although the increase in axial detector length increases sensitivity, it also increases the adverse effects of parallax errors as observed with traditional detectors. Parallax errors occur when an annihilation photon enters one crystal element but is absorbed after penetrating an adjacent crystal element. This error generally occurs for high oblique angles of incidence. Parallax errors may be reduced if detectors are equipped with depth-of-interaction information (30,31).
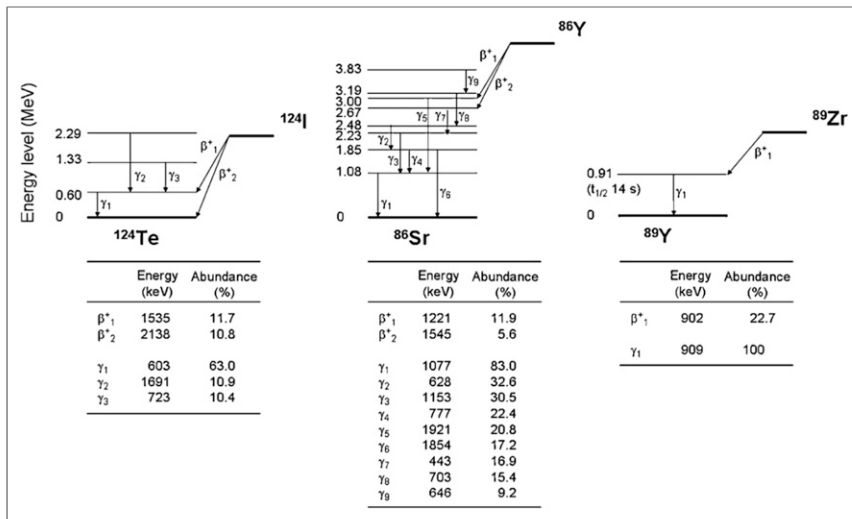
FIGURE 4. Decay scheme of several isotopes that emit prompt γ-rays in cascade with positron emission (59).

Reconstruction. Advances in image reconstruction include modeling of motion by incorporating information on motion into the reconstruction algorithm (32,33). Motion correction can easily be performed by including counts from only a certain phase of the respiratory cycle (e.g., end expiration). Such a phase-gated approach suffers, however, from prolonged scan times (or increased noise) because of loss of the data that are discarded for reconstruction. Correction for respiratory motion may be implemented using information on motion from additional hardware (e.g., a belt system). However, similar results can also be obtained with data-driven approaches (34) without the use of additional hardware. Event-by-event motion correction is an approach in which all data are used to reconstruct an image (35,36). This approach leads to less noise than phase-gated

motion correction. In general, reconstruction algorithms with motion correction often use data that were acquired in list mode. Acquiring data in list mode means that for each count the time and position of detection are stored. List-mode acquisitions are especially useful for motion-corrected reconstruction algorithms, because retrospective redefinition of phases in phase-gated sinograms is allowed.

Like SPECT images, PET images may be improved by integrating anatomic information in the reconstruction algorithm using anatomic priors (37,38). In addition to using anatomic priors, smoothing priors can be incorporated with a penalty term that suppresses noise (39,40).

For some isotopes, positrons are emitted in cascade with the emission of other γ-photons, so that additional photons are emitted together with the 2 annihilation photons (Fig. 4). These additional photons are called prompt γ-photons. ^{124}I and ^{86}Y are examples of isotopes that emit prompt γ-photons in cascade with the positron and are often used for matched-pairs dosimetry of the therapeutic isotopes ^{131}I and ^{90}Y, respectively (41). When these prompt γ-photons are detected, they may be mistaken for an annihilation photon, resulting in an erroneous line of response. The adverse effects of the prompt γ-photons can be corrected for by implementing a prompt γ-correction in the reconstruction algorithm (42,43).

PET/MRI. PET/MRI has several advantages over PET/CT, of which higher soft-tissue contrast is probably most important for treatment planning, dosimetry, and assessment of response to radionuclide therapies. Additionally, the simultaneous acquisition of coregistered MR images may benefit accurate dosimetry. Also, MRI can be used to identify organs at risk (or parts of one organ), which may be essential for determining the maximum tolerable radionuclide dosage. Moreover, the simultaneous acquisition of anatomic and molecular images enables accurate motion correction—for instance, by making real-time MR images of the lungs.

The integration of PET and MRI modalities does, however, bring about serious challenges, because mutual interference between modalities can occur. That is, photomultiplier tubes used in traditional PET detectors do not function in the strong magnetic fields used for MRI. Moreover, the radiofrequency
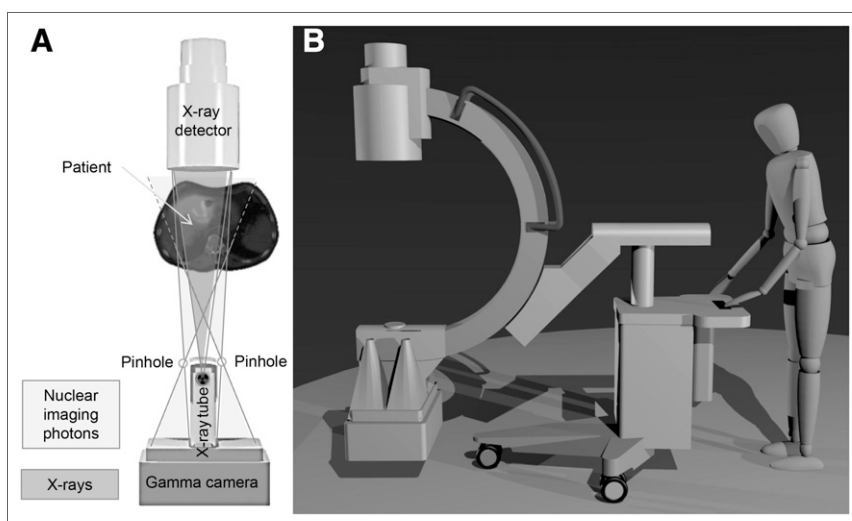

FIGURE 5. (A) Hybrid C-arm showing field of view of pinhole collimator and x-ray photons. (B) Entire system (50).
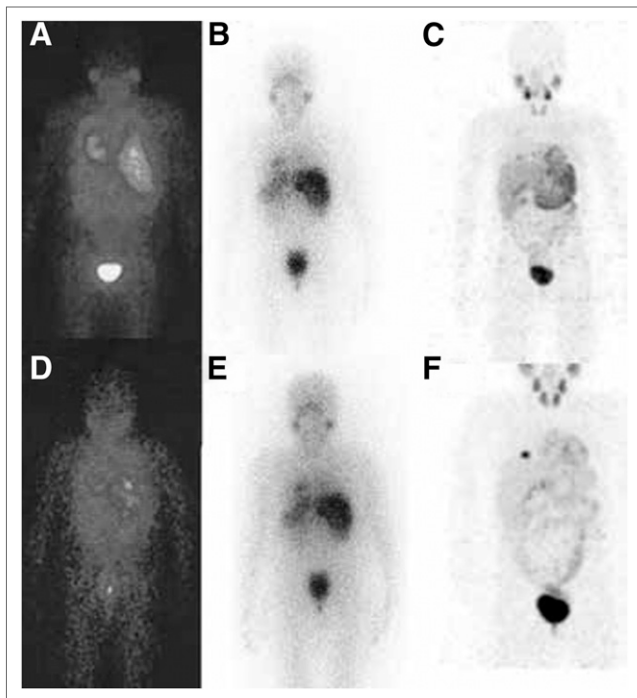
FIGURE 6. Diagnostic ¹²³I-MIBG planar acquisitions at 4 h (A) and 24 h (D) after injection, posttherapy ¹³¹I-MIBG planar acquisitions at 24 h (B) and 48 h (E) after injection, and ¹²⁴I-MIBG maximum-intensity-projection acquisitions at 24 h (C) and 48 h (F) after injection (*51*). Resolution advantage of ¹²⁴I PET over ¹²³I and ¹³¹I SPECT is clear.

signal used for MRI is affected by the PET modules (*44*). For this reason, the first generation of PET/MRI systems acquired PET and MR images in sequence and the modalities were spatially separated. Integrated systems in which the PET detectors are inserted into the bore of the MR scanner are now available so that PET and MR images can be acquired simultaneously. Integrated PET/MRI systems use detector systems based on either avalanche photodiodes or SiPMs that are insensitive to the magnetic field. The simultaneous measurement ensures a better spatial agreement of PET and MRI data and provides a unique opportunity for 4-dimensional acquisitions—for example, to perform motion correction without the need for respiratory motion sensors.

Disadvantages of PET/MRI include the high costs and the fact that ferromagnetic metallic implants are contraindications for MRI. Moreover, one of the big challenges for PET/MRI is attenuation correction. Accurate attenuation correction is required for quantitative PET/MRI, which is important for dosimetry in radionuclide therapy. CT images are ideal for attenuation correction as they provide electron-density images, whereas MR images give information about proton density, making them less suitable for attenuation correction. Moreover, MR images are often transaxially truncated. Despite the challenges in MR-based attenuation correction, segmentation-based or template- or atlas-based techniques can be used to derive electron density information from MR images (*45*). Alternatively, the attenuation maps may be estimated using algorithms that use the time-of-flight emission or transmission data (*46*).

OTHER MODALITIES FOR GUIDANCE

Imaging modalities other than nuclear imaging are also used to guide radionuclide therapy. For example, fluoroscopic imaging is used for radionuclide therapies that require real-time image guidance, such as assisting in the positioning of catheters for liver radioembolization (*47*). With the development of interventional MRI scanners, these procedures may also be performed in the future under MRI guidance for increased soft-tissue contrast and the absence of radiation dose. Intratumoral injection of radionuclides may also be performed under guidance from interventional CT images or using ultrasound (*48,49*).

FUTURE PERSPECTIVES

Simultaneous X-Ray and Nuclear Imaging

To date, no real-time hybrid imaging modalities for interventional purposes have been developed that combine simultaneously acquired nuclear and anatomic images. Fluoroscopic imaging in conjunction with real-time nuclear imaging would provide the physician with valuable information during procedures such as ⁹⁰Y liver radioembolization by imaging the distribution of the radionuclide in relation to the anatomy and the interventional instruments, thereby improving therapeutic efficiency.
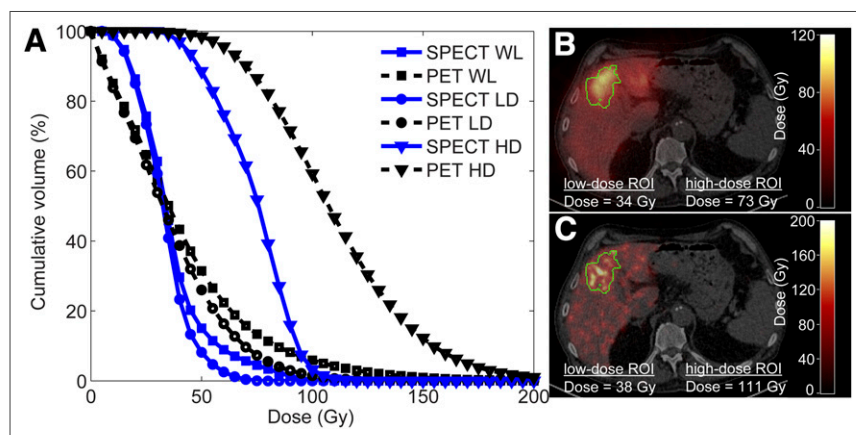

FIGURE 7. Comparison of dose estimates based on ⁹⁰Y PET and ⁹⁰Y SPECT images after radioembolization procedure. (A) Graph shows cumulative dose–volume histogram of whole liver (WL), low-dose region of interest (LD), and high-dose region of interest (HD). (B and C) Same transversal slice through SPECT-based dose map fused with CT (B) and through PET-based dose map (C) (*60*) shows advantage of PET over SPECT in terms of resolution and effect on calculated dose distribution.

Imaging of the same field of view can be achieved by placing an x-ray tube, an x-ray detector, and a γ-camera in one line (50). Since straightforward combination of these elements would block the line of views, a γ-camera geometry that looks around the x-ray tube was developed. A prototype was built using a mobile C-arm and a γ-camera with a 4-pinhole collimator. Measurements with the hybrid-imaging prototype that combines simultaneous x-ray and nuclear imaging of the same field of view have demonstrated the feasibility of real-time simultaneous hybrid imaging in the intervention room (Fig. 5).

PET Versus SPECT

Generally, SPECT is less expensive than PET in the sense of initial investment and isotopes. However, PET outperforms SPECT with respect to sensitivity, resolution, and quantitative capabilities. One approach to improving the quality of nuclear images is therefore to replace SPECT tracers with positron-emitting PET tracers. Examples include the use of diagnostic ^{124}I-metaiodobenzylguanidine (MIBG) PET instead of ^{123}I-MIBG SPECT before ^{131}I-MIBG therapy (51,52) (Fig. 6) or the use of low-abundance internal pair production of ^{90}Y for ^{90}Y PET instead of Bremsstrahlung ^{90}Y SPECT for dosimetry in ^{90}Y liver radioembolization (Fig. 7) (53).

These advances spur the question of whether there is a future for SPECT systems in the nuclear medicine department. Some have argued that PET may completely replace scintigraphy and SPECT in the future (54). However, the type of decay determines whether SPECT or PET is used for imaging. Finding suitable and cost-effective positron-emitting alternatives with a half-life long enough for dosimetry remains a challenge for many SPECT radiopharmaceuticals. Moreover, both PET imaging and SPECT imaging are often applied for theranostics, using matched pairs of isotopes to exploit the characteristics of the PET isotopes that are most suitable for imaging (^{124}I and ^{86}Y) and their β-emitting counterparts (^{131}I and ^{90}Y) for therapeutic purposes (41). This is referred to as matched-pairs dosimetry. For example, ^{124}I is used for pretherapeutic imaging of suspected recurrence of differentiated thyroid carcinoma, because a low activity of ^{124}I (∼1% of therapeutic ^{131}I activity) is often sufficient to achieve similar image quality on pretherapeutic ^{124}I PET/CT and posttherapeutic ^{131}I SPECT/CT (55). Another example is the use of ^{86}Y PET before ^{90}Y therapy of somatostatin receptor–positive tumors (56), which has been shown to improve image quality as compared with ^{111}In SPECT (57).

With developments such as matched-pairs dosimetry, SPECT and PET are likely to be used for many years to come because of the complementary capabilities of PET and SPECT radionuclides.

CONCLUSION

As the quality of the images used for guidance of radionuclide therapy are continuously improved, the outcome and efficiency of radionuclide therapies may also be improved. For example, improved pretherapeutic image quality may lead to improved patient selection and, subsequently, to increased accuracy of required dose estimates, paving the way for dosimetry-guided individualized doses. In turn, this development would have the potential to reduce the occurrence of side effects and increase the probability of a successful ablation of the tumor. Technical advances that benefit imaging in radionuclide therapy include developments in algorithms and instrumentation for traditional nuclear imaging modalities, as well as the development of novel modalities.

DISCLOSURE

No potential conflict of interest relevant to this article was reported.

REFERENCES

1. Kwekkeboom DJ, de Herder WW, Kam BL, et al. Treatment with the radiolabeled somatostatin analog [^{177}Lu-DOTA^0,Tyr^3]octreotate: toxicity, efficacy, and survival. *J Clin Oncol.* 2008;26:2124–2130.
2. Seidlin SM, Marinelli LD, Oshry E. Radioactive iodine therapy: effect on functioning metastases of adenocarcinoma of the thyroid. *J Am Med Assoc.* 1946;132:838–847.
3. Smits MLJ, Prince JF, Rosenbaum CENM, et al. Intra-arterial radioembolization of breast cancer liver metastases: a structured review. *Eur J Pharmacol.* 2013;709:37–42.
4. Ogawa K, Harata Y, Ichihara T, Kubo A, Hashimoto S. A practical method for position-dependent Compton-scatter correction in single photon emission CT. *IEEE Trans Med Imaging.* 1991;10:408–412.
5. Zeng GL, Gullberg GT, Tsui BMW, Terry JA. Three-dimensional iterative reconstruction algorithms with attenuation and geometric point response correction. *IEEE Trans Nucl Sci.* 1991;38:693–702.
6. Walrand S, Hesse M, Wojcik R, Lhommel R, Jamar F. Optimal design of Anger camera for bremsstrahlung imaging: Monte Carlo evaluation. *Front Oncol.* 2014;4:149.
7. Schramm NU, Ebel G, Engeland U, Schurrat T, Behe M, Behr TM. High-resolution SPECT using multipinhole collimation. *IEEE Trans Nucl Sci.* 2003;50:315–320.
8. Beijst C, Elschot M, Viergever MA, de Jong HWAM. A parallel-cone collimator for high-energy SPECT. *J Nucl Med.* 2015;56:476–482.
9. Sharir T, Slomka PJ, Berman DS. Solid-state SPECT technology: fast and furious. *J Nucl Cardiol.* 2010;17:890–896.
10. Melis M, de Swart J, de Visser M, et al. Dynamic and static small-animal SPECT in rats for monitoring renal function after ^{177}Lu-labeled Tyr3-octreotate radionuclide therapy. *J Nucl Med.* 2010;51:1962–1968.
11. Kojima A, Gotoh K, Shimamoto M, Hasegawa K, Okada S. Iodine-131 imaging using 284 keV photons with a small animal CZT-SPECT system dedicated to low-medium-energy photon detection. *Ann Nucl Med.* 2016;30:169–175.
12. van Gils CAJ, Beijst C, van Rooij R, et al. Impact of reconstruction parameters on quantitative I-131 SPECT. *Phys Med Biol.* 2016;61:5166–5182.
13. Elschot M, Smits MLJ, Nijsen JFW, et al. Quantitative Monte Carlo-based holmium-166 SPECT reconstruction. *Med Phys.* 2013;40:112502–112512.
14. De Jong HWAM, Slijpen TP, Beekman FJ. Acceleration of Monte Carlo SPECT simulation using convolution-based forced detection. *IEEE Trans Nucl Sci.* 2001;48:58–64.
15. Beekman FJ, De Jong HW, Van Geloven S. Efficient fully 3-D iterative SPECT reconstruction with Monte Carlo-based scatter compensation. *IEEE Trans Med Imaging.* 2002;21:867–877.
16. Bailey DL, Willowson KP. Quantitative SPECT/CT: SPECT joins PET as a quantitative imaging modality. *Eur J Nucl Med Mol Imaging.* 2014;41(suppl 1):S17–S25.
17. Dewaraja YK, Frey EC, Sgouros G, et al. MIRD pamphlet no. 23: quantitative SPECT for patient-specific 3-dimensional dosimetry in internal radionuclide therapy. *J Nucl Med.* 2012;53:1310–1325.
18. Akabani G, Hawkins WG, Eckblade MB, Leichner PK. Patient-specific dosimetry using quantitative SPECT imaging and three-dimensional discrete Fourier transform convolution. *J Nucl Med.* 1997;38:308–314.

19. Lehovich A, Bruyant PP, Gifford HS, et al. Impact on reader performance for lesion-detection/localization tasks of anatomical priors in SPECT reconstruction. *IEEE Trans Med Imaging.* 2009;28:1459–1467.

20. Reader AJ, Verhaeghe J. 4D image reconstruction for emission tomography. *Phys Med Biol.* 2014;59:R371–R418.

21. Zaidi H, Montandon M-L. Scatter compensation techniques in PET. *PET Clin.* 2007;2:219–234.

22. Casey ME, Hoffman EJ. Quantitation in positron emission computed tomography: 7. A technique to reduce noise in accidental coincidence measurements and coincidence efficiency calibration. *J Comput Assist Tomogr.* 1986;10:845–850.

23. Slomka PJ, Pan T, Germano G. Recent advances and future progress in PET instrumentation. *Semin Nucl Med.* 2016;46:5–19.

24. Surti S. Update on time-of-flight PET imaging. *J Nucl Med.* 2015;56:98–105.

25. Conti M. Improving time resolution in time-of-flight PET. *Nucl Instrum Methods Phys Res A.* 2011;648(suppl):S194–S198.

26. Moses WW, Janecek M, Spurrier MA, et al. Optimization of a LSO-based detector module for time-of-flight PET. *IEEE Trans Nucl Sci.* 2010;57:1570–1576.

27. Seifert S, Schaart DR. Improving the time resolution of TOF-PET detectors by double-sided readout. *IEEE Trans Nucl Sci.* 2015;62:3–11.

28. Jakoby BW, Bercier Y, Watson CC, Bendriem B, Townsend DW. Performance characteristics of a new LSO PET/CT scanner with extended axial field-of-view and PSF reconstruction. *IEEE Trans Nucl Sci.* 2009;56:633–639.

29. Poon JK, Dahlbom ML, Moses WW, et al. Optimal whole-body PET scanner configurations for different volumes of LSO scintillator: a simulation study. *Phys Med Biol.* 2012;57:4077–4094.

30. Ito M, Hong SJ, Lee JS. Positron emission tomography (PET) detectors with depth-of-interaction (DOI) capability. *Biomed Eng Lett.* 2011;1:70–81.

31. Schmall JP, Karp JS, Werner M, Surti S. Parallax error in long-axial field-of-view PET scanners: a simulation study. *Phys Med Biol.* 2016;61:5443–5455.

32. Rahmim A, Rousset O, Zaidi H. Strategies for motion tracking and correction in PET. *PET Clin.* 2007;2:251–266.

33. Rahmim A, Tang J, Zaidi H. Four-dimensional (4D) image reconstruction strategies in dynamic PET: beyond conventional independent frame reconstruction. *Med Phys.* 2009;36:3654–3670.

34. Büther F, Vehren T, Schäfers KP, Schäfers M. Impact of data-driven respiratory gating in clinical PET. *Radiology.* 2016;281:229–238.

35. Liu C, Alessio AM, Kinahan PE. Respiratory motion correction for quantitative PET/CT using all detected events with internal-external motion correlation. *Med Phys.* 2011;38:2715–2723.

36. Chan C, Jin X, Fung EK, et al. Event-by-event respiratory motion correction for PET with 3D internal-1D external motion correlation. *Med Phys.* 2013;40:112507.

37. Cheng-Liao J, Qi J. PET image reconstruction with anatomical edge guided level set prior. *Phys Med Biol.* 2011;56:6899–6918.

38. Bowsher JE, Johnson VE, Turkington TG, Jaszczak RJ, Floyd CR, Coleman RE. Bayesian reconstruction and use of anatomical a priori information for emission tomography. *IEEE Trans Med Imaging.* 1996;15:673–686.

39. Fessler JA, Hero AO. Penalized maximum-likelihood image reconstruction using space-alternating generalized EM algorithms. *IEEE Trans Image Process.* 1995;4:1417–1429.

40. Hebert T, Leahy R. A generalized EM algorithm for 3-D Bayesian reconstruction from Poisson data using Gibbs priors. *IEEE Trans Med Imaging.* 1989;8:194–202.

41. Lopci E, Chiti A, Castellani MR, et al. Matched pairs dosimetry: ^{124}I/^{131}I meta-iodobenzylguanidine and ^{124}I/^{131}I and ^{86}Y/^{90}Y antibodies. *Eur J Nucl Med Mol Imaging.* 2011;38(suppl 1):S28–S40.

42. Beattie BJ, Finn RD, Rowland DJ, Pentlow KS. Quantitative imaging of bromine-76 and yttrium-86 with PET: a method for the removal of spurious activity introduced by cascade gamma rays. *Med Phys.* 2003;30:2410–2423.

43. Surti S, Scheuermann R, Karp JS. Correction technique for cascade gammas in I-124 imaging on a fully-3D, time-of-flight PET scanner. *IEEE Trans Nucl Sci.* 2009;56:653–660.

44. Torigian DA, Zaidi H, Kwee TC, et al. PET/MR imaging: technical aspects and potential clinical applications. *Radiology.* 2013;267:26–44.

45. Keereman V, Mollet P, Berker Y, Schulz V, Vandenberghe S. Challenges and current methods for attenuation correction in PET/MR. *MAGMA.* 2013;26:81–98.

46. Nuyts J, Dupont P, Stroobants S, Benninck R, Mortelmans L, Suetens P. Simultaneous maximum a posteriori reconstruction of attenuation and activity distributions from emission sinograms. *IEEE Trans Med Imaging.* 1999;18:393–403.

47. Kennedy AS, Salem R. Radioembolization (yttrium-90 microspheres) for primary and metastatic hepatic malignancies. *Cancer J.* 2010;16:163–175.

48. Tian JH, Xu BX, Zhang JM, Dong BW, Liang P, Wang XD. Ultrasound-guided internal radiotherapy using yttrium-90-glass microspheres for liver malignancies. *J Nucl Med.* 1996;37:958–963.

49. Phillips WT, Bao A, Brenner AJ, Goins BA. Image-guided interventional therapy for cancer with radiotherapeutic nanoparticles. *Adv Drug Deliv Rev.* 2014;76:39–59.

50. Beijst C, Elschot M, Viergever MA, de Jong HWAM. Toward simultaneous real-time fluoroscopic and nuclear imaging in the intervention room. *Radiology.* 2016;278:232–238.

51. Cistaro A, Quartuccio N, Caobelli F, et al. ^{124}I-MIBG: a new promising positron-emitting radiopharmaceutical for the evaluation of neuroblastoma. *Nucl Med Rev Cent East Eur.* 2015;18:102–106.

52. Beijst C, de Keizer B, Lam MGEH, Janssens GO, Tytgat GAM, de Jong HWAM. A phantom study: should ^{124}I-mIBG PET/CT replace ^{123}I-mIBG SPECT/CT? *Med Phys.* 2017;44:1624–1631.

53. Kao Y-H, Steinberg JD, Tay Y-S, et al. Post-radioembolization yttrium-90 PET/CT—part 1: diagnostic reporting. *EJNMMI Res.* 2013;3:56.

54. Alavi A, Basu S. Planar and SPECT imaging in the era of PET and PET-CT: can it survive the test of time? *Eur J Nucl Med Mol Imaging.* 2008;35:1554–1559.

55. Beijst C, Kist JW, Elschot M, et al. Quantitative comparison of ^{124}I PET/CT and ^{131}I SPECT/CT detectability. *J Nucl Med.* 2016;57:103–108.

56. Pauwels S, Barone R, Walrand S, et al. Practical dosimetry of peptide receptor radionuclide therapy with ^{90}Y-labeled somatostatin analogs. *J Nucl Med.* 2005;46(suppl 1):92S–98S.

57. Helisch A, Förster GJ, Reber H, et al. Pre-therapeutic dosimetry and biodistribution of ^{86}Y-DOTA-Phe1-Tyr3-octreotide versus ^{111}In-pentetreotide in patients with advanced neuroendocrine tumours. *Eur J Nucl Med Mol Imaging.* 2004;31:1386–1392.

58. Walrand S, Hesse M, Demonceau G, Pauwels S, Jamar F. Yttrium-90-labeled microsphere tracking during liver selective internal radiotherapy by bremsstrahlung pinhole SPECT: feasibility study and evaluation in an abdominal phantom. *EJNMMI Res.* 2011;1:32.

59. Lubberink M, Herzog H. Quantitative imaging of ^{124}I and ^{86}Y with PET. *Eur J Nucl Med Mol Imaging.* 2011;38(suppl 1):S10–S18.

60. Elschot M, Vermolen BJ, Lam MGEH, de Keizer B, van den Bosch MAAJ, de Jong HWAM. Quantitative comparison of PET and Bremsstrahlung SPECT for imaging the in vivo yttrium-90 microsphere distribution after liver radioembolization. *PLoS One.* 2013;8:e55742.